Journal of Materials Chemistry A

Boron-Doped Coronenes with High Redox Potential for Organic Positive Electrodes in Lithium-Ion Batteries: First-Principles Density Functional Theory Modeling Study

Journal:	*Journal of Materials Chemistry A*
Manuscript ID	TA-ART-02-2018-001671.R2
Article Type:	Paper
Date Submitted by the Author:	26-Apr-2018
Complete List of Authors:	Zhu, Yuntong; University of Science and Technology Beijing, Department of Inorganic Nonmetallic Materials Kim, Ki Chul; Konkuk University, Chemical Engineering Jang, Seung Soon; Georgia Institute of Technology, School of Materials Science and Engineering

Journal of Materials Chemistry A

ARTICLE

Boron-Doped Coronenes with High Redox Potential for Organic Positive Electrodes in Lithium-Ion Batteries: First-Principles Density Functional Theory Modeling Study

Received 00th January 20xx,
Accepted 00th January 20xx

DOI: 10.1039/x0xx00000x

www.rsc.org/

Yuntong Zhu,[a] Ki Chul Kim*[b] and Seung Soon Jang*[acd]

Boron-doped coronenes are attractive as promising positive electrode materials for lithium-ion batteries due to the unique physical and chemical properties of coronene. In this study, we computationally investigate the thermodynamics and redox properties of the boron-doped coronenes using the first-principles density functional theory method to evaluate their potential for positive electrodes. It is found from our computations that the redox potentials of the boron-doped coronenes are changed as a function of the number of doped boron atoms and their distribution, predicting that the weight-averaged redox potentials of one-boron- and two-boron-doped coronenes would attain 5.30 V and 2.23 V, respectively, with respect to Li/Li^+. It is highlighted that the highest redox potential of 5.42 V vs. Li/Li^+ is predicted for the coronene with a boron atom doped at an edge position. Further investigation on the electronic properties of the boron-doped coronenes provides a strong correlation of the redox potential with the electron affinity, but poor correlation with the lowest unoccupied molecular orbital. Last, a proposed synthetic route that utilizes the pristine coronene reacting with B_2O_3 and Mg for developing boron-doped-coronenes provides viable thermodynamic conditions of the released CO pressures of ~1.3×10^{-6} atm at 1073 K and ~2.8×10^{-5} atm at 1273 K.

Introduction

Modern society has an increasing concern on environmental pollution and global warming owing to the excessive use of limited fossil fuels. To mitigate their negative effects on the environment and to preserve natural resources, various alternative energy generation technologies, such as wind energy, wave energy, and solar energy, have been developed and implemented in the last two decades.[1-4] Yet, the intermittent characteristics of these sustainable energy technologies require advanced energy storage devices to stably offer electricity for stationary power plant applications.[1-4, 6-9] Besides, increasing demands on electric vehicles and portable electronic devices have attracted tremendous attentions to developing electrochemical energy storage technologies with high cell performance including their fast response and easy modularization as well as the high energy, charge, and power capacities.[1, 3, 4, 6, 9-12] Among available candidates, lithium-ion batteries are a class of promising secondary batteries owing to their high energy and charge capacities in addition to the cyclic stability.[2-4, 6-10] However, the current lithium ion batteries suffer from several bottlenecks that hinder their widespread utilization. Difficulty in the diffusion of lithium ions through the bulk phase of conventional transition metal oxides for positive electrodes is a major problem that results in the poor power capacities of the lithium-ion batteries.[3, 7] To overcome this problem and make remarkable progress, it is necessary to design novel positive electrode materials with enhanced ionic diffusivities without compensating for the high charge and energy densities.[3, 4, 6, 7] The designed materials are, therefore, expected to meet the following critical conditions: (1) high cell voltages, (2) enhanced power capacities, (3) excellent charge and energy capacities. Recent progresses realizing these three conditions have primarily focused on transition metal oxides, such as $LiCoO_2$, $LiMn_2O_4$, $LiFePO_4$, and Li_2FeSiO_4.[1, 13-18] However, enhanced approaches still need to be developed to make a breakthrough progress in the positive electrodes.

Recently, organic materials have gained widespread interest owing to the light weight and cost effectiveness that can be obtained by replacing expensive transition metal oxides with abundantly available carbon-based materials.[10, 19] In particular, graphene and its derivatives with highly accessible inner spaces have been investigated as potential positive electrodes in lithium-ion batteries[9, 12, 20, 21] due to their unique physical and chemical properties as well as scalable synthetic methods (e.g., revised Hummer's method and chemical vapor deposition).[22, 23] Nonetheless, these studies showed that poor Li-binding behaviors with pristine graphene made them

[a] Computational NanoBio Technology Laboratory, School of Materials Science and Engineering, Georgia Institute of Technology, Atlanta, GA 30332-0245, USA. E-mail: seungsoon.jang@mse.gatech.edu
[b] Department of Chemical Engineering, Konkuk University, Seoul 05029, the Republic of Korea. E-mail: kich2018@konkuk.ac.kr
[c] Institute for Electronics and Nanotechnology, Georgia Institute of Technology, Atlanta, GA 30332, USA.
[d] Parker H. Petit Institute for Bioengineering and Bioscience, Georgia Institute of Technology, Atlanta, GA 30332, USA.

Electronic Supplementary Information [5] available: The structure and spin states for the B2-3 case as a representative example. Figure S1. Tables S1-S3. See DOI: 10.1039/x0xx00000x

inapplicable for positive electrode materials in lithium-ion battery.[24, 25]

To overcome the major problem, extensive efforts have been paid to improve the Li-binding strength and charge storage capacity by systematically modifying graphene surfaces. Various intrinsic defects, such as mono-vacancy, di-vacancy, and Stone-Wales, have been considered to modify the graphene surfaces with the aim of altering the electronic properties of the surfaces and thereby improving the Li-binding strength.[26-28] However, imprecise manipulation of vacancy sizes and types in reality may lead to the unstable and unpredictable behaviors of resultant materials, which may cause undesirable degradation in cell performance.

On the other hand, alternative approaches, such as adding functional groups[9, 12] and substituting carbon with hetero-atoms like boron and nitrogen,[24, 29-32] have been employed to modify graphene. For instance, Liu et al. studied the redox properties of hydrothermally reduced graphene oxides as positive electrodes.[12] They reported that the functionalization of the graphene with carbonyl and epoxide groups could improve both the redox potential and charge capacity. Uthaisar et al. investigated the influence of oxygen-containing groups on the electronic properties of the graphene nanoribbons. They suggested that ketone groups terminating the edges would play a dramatic role in the electrochemical interaction of Li with the graphene nanoribbons.[33] In addition, the previous studies showed that the capacity of boron-doped graphene could be substantially improved as compared with the pristine graphene[20, 24] while preserving its good structural integrity owing to the comparable sizes of boron and carbon.[34] Wu et al. reported that a reversible capacity of 1549 mAh/g could be achieved by boron-doped graphenes.[20] Hardikar et al. studied the diffusion kinetics of Li across the basal planes of boron-doped defective graphenes,[24] suggesting that a low adsorption energy barrier and enhanced Li adsorption could be attained in a boron-doped mono-vacancy graphene. These studies emphasize the potential of boron-doped graphene as promising positive electrode materials in lithium-ion batteries. However, despite these efforts, understanding on the correlation of the redox properties of boron-doped graphene with their doping patterns remains unclear to be explored. Thus, systematic investigations on the redox properties of boron-doped graphene with varied dopant configurations are essential to design promising graphene-based materials for the applications to positive electrodes.

Manzhos and coworkers previously studied the electronic and redox properties of various organic electrode materials, such as coronene and phenalene.[35] In their study, the authors doped a pristine coronene with one or three boron atoms at its center and assessed the potential of the materials as positive electrodes for lithium- and sodium-ion batteries. In this paper, we designed a broad array of one- and two-boron-doped coronene models to accomplish a boron-doping strategy for the coronene. Specifically, we employed coronenes ($C_{24}H_{12}$) as a model system of graphene flakes and investigated the thermodynamics and redox properties for a series of boron-doped coronenes with various concentrations and positions of doped boron atoms as shown in Figure 1. Density functional theory (DFT) modeling approach was used to efficiently evaluate their potential as positive electrodes. It was highlighted that one- and two-boron-doped coronenes exhibited high and moderate weight-averaged redox potentials of 5.30 V and 2.23 V with respect to Li/Li^+, respectively, which would demonstrate their suitability as positive electrode. For better understanding of these redox properties, we analyzed the correlations of their redox potentials with the electronic properties. Finally, a scalable synthetic route with viable thermodynamic conditions (temperature and pressure) for boron-doped coronenes was discussed. Note that the primary scope of this study is to understand the effect of the boron doping on the redox properties of coronenes. Thus, the study on the Li-binding properties of a selected set of coronene derivatives with the aim of assessing their potential use in lithium-ion batteries will be pursued in future.

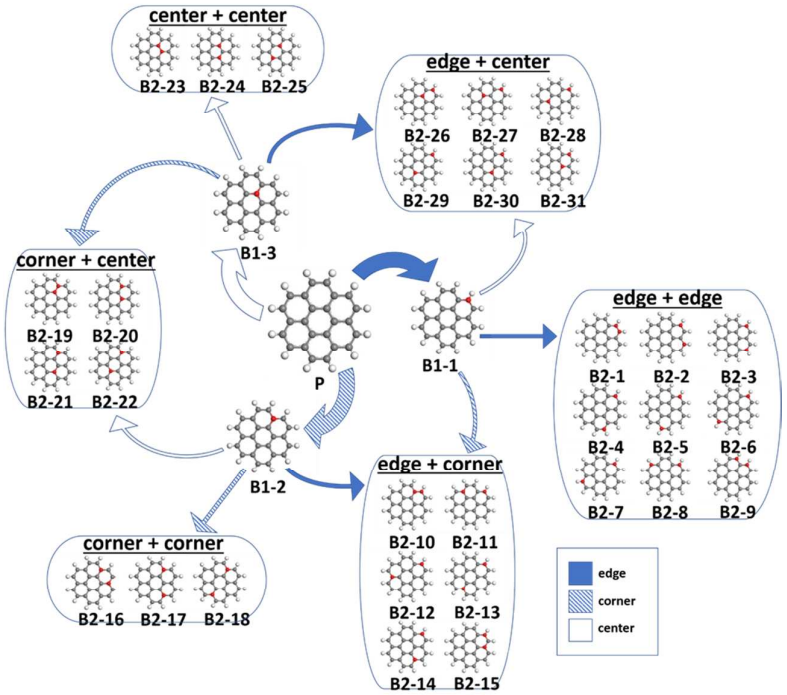

Figure 1. Systematic introduction of one and two boron dopants into coronene. Here, "P" represents the pristine coronene while boron-doped coronenes are depicted by "Bm-n" with m and n indicating the number of boron dopants and the case number, respectively. Arrows in dark blue, light blue, and white represent dopants introduced at the edge, corner, and center of the molecule, respectively. The 31 two-boron-doped coronene molecules are categorized depending on the position of the second boron dopant.

Computational methods

Redox potential and electronic properties

In this study, the redox potential is evaluated by the intrinsic electrochemical potential of the material itself with respect to counter electrode. All the calculations to compute redox potentials of coronene derivatives were performed using the DFT method implemented in Jaguar software.[36] Exchange and correlation interactions were estimated by using PBE0 functional[37, 38] and 6-31+G(d,p) basis set was used to describe molecular orbitals.[39] The redox potentials of boron-doped coronenes in solution phase were calculated using the thermodynamic cycle suggested by Truhlar et al.[40, 41] as described in Figure 2. Note that our previous studies have verified that this computational approach provides accurate predictions for redox potentials in a great agreement with experimental values.[9, 10, 12, 42, 43] The reduction free energy in solution phase ($\Delta G^{red}(R, sol)$) can be written as

$$\Delta G^{red}(R, sol) = \Delta G^{red}(R, gas) + \Delta G^{solv}(R^-) - \Delta G^{solv}(R) \quad (1)$$

where $\Delta G^{red}(R, gas)$, $\Delta G^{solv}(R^-)$, and $\Delta G^{solv}(R)$ are the free energy change of a molecule for reduction in gas phase with vibrational contributions at 298.15 K, the solvation free energy change of the molecule in anionic state, and the solvation free energy change of the molecule in neutral state, respectively. The Poisson-Boltzmann model[44] was used to calculate the solvation free energies for both neutral and anionic states. The dielectric constant of 16.14 was used to represent the mixture of ethylene carbonate and dimethyl carbonate with the molar ratio of 3:7. The implicit solvent model was applied in our previous studies to investigate the redox properties of various quinone derivatives,[9, 10, 12, 42, 43] demonstrating that the redox potentials calculated based on this solvent model were in a great agreement with the experimental values within an uncertainty of <0.2 V vs. Li/Li^+.[10] Therefore, it is believed that the solvent model is appropriate for studying redox properties for general organic materials, including boron-doped coronenes in this work. Also, note that the coronene molecules introduced in this study are assumed to be fully solvated by solvent molecules. This would allow us to use the implicit solvent model of the mixed solvents with the dielectric polarization constant of 16.14. However, we might be curious about the redox potentials of the coronene molecules under a condition where they aggregate themselves to form molecular solid, meaning that a considerable number of coronene molecules are sterically hindered by neighboring coronene molecules without contacting solvent molecules directly. In this situation, the applied dielectric polarization constant would be different from 16.14. Regarding this, we previously studied the correlation of the redox potential with various dielectric polarization constant.[10] Based on the previous study, we think that it would be possible to predict the redox potentials of coronene derivatives by considering the dielectric environment consisting of various concentrations of coronene-based molecular solids.

For each molecule, we checked the stability of the spin multiplicity by considering its spin state from singlet to quartet state, and then the most stable spin state was utilized for further calculations. Table S1 summarizes the most stable spin multiplicities for the pristine coronene and its boron-doped derivatives at the neutral and anionic charge states.

Then, the redox potential in solution phase with respect to Li/Li^+ was calculated based on the free energy change for reduction in solution phase using the following equation:

$$E^o_{w.r.t.Li} = \left(-\frac{\Delta G^{red}(S,\ sol)}{nF} - E_H\right) - E_{Li} \quad (2)$$

where *n* represents the number of electrons transferred, *F* represents the Faraday constant (96485 C/mol), E_H represents the redox potential of the hydrogen electrode (4.44 V),[45] and E_{Li} represents the redox potential of the Li electrode with respect to the standard hydrogen electrode (-3.05 V).[46] The adiabatic electron affinity was employed to calculate the electron affinity of each coronene derivative. The spin density for each atom in boron-doped coronenes is computed by the Mulliken population analysis.

Note that other computational approach utilizing the reaction scheme has been also reported to calculate the redox potentials of materials. However, this approach usually requires the accurate information of the product such as lithiated structure and thereby this approach has been rigorously utilized for predicting the redox potentials of inorganic cathode materials having the accurate information on positions of lithium ions placed in the materials. Thus, our approach evaluated by the intrinsic electrochemical potential of material itself with respect to counter electrode would be very useful for predicting the redox potentials of the organic materials that do not have clear information on lithiated structures. The reaction-scheme-based approach predicted the redox potential of 2.34 V vs. Li/Li^+ for the B1-2 case which was significantly lower than the value (5.30 V vs. Li/Li^+) predicted by our computational approach. Although we need to further investigate the difference between these two approaches in future, this difference should be made by the geometrical change after Li binding.

Further, please note that the coronene derivatives can be chemically bound onto conductive carbon materials, such as graphenes and carbon nanotubes, which would be a strategy to use the coronene derivatives in cathodes by preventing the molecular dissolution. Polymerization is another strategy to resolve this issue. Liu et al. demonstrated the high cycling stability with self-polymerized dopamines which were spontaneously coated on the surfaces of few-walled carbon nanotubes, indicating the successful incorporation of organic molecules in cathodes.[42]

Relative thermodynamic stability and weight-averaged redox potential

The Boltzmann factor was used to assess the relative thermodynamic stability of boron-doped-coronenes with a specific number of boron dopants. For a group of either one-boron-doped (3 configurations) or two-boron-doped (31 configurations) coronenes, the Boltzmann factor (F_i) of the i^{th} configuration was obtained by

$$F_i = \exp(-\frac{G_{sol}}{k_b T}) \quad (3)$$

where G_{sol} is the Gibbs free energy in solution phase obtained by the DFT calculation, k_b is the Boltzmann constant, and T is the absolute temperature (298.15 K). Based on the calculated Boltzmann factors, the relative probability estimating the presence of the i^{th} configuration (p_i) was computed by

$$p_i = \frac{F_i}{\sum_i F_i} \quad (4)$$

where $\sum_i F_i$ is the sum of the Boltzmann factors for all the configurations with a specific number of boron dopants. Weight-averaged redox potential for a group of either one- or two-boron-doped coronenes ($E^o_{avg,w.r.t.Li}$) was finally predicted by

$$E^o_{avg\ w.r.t.Li} = \sum_i p_i E^o_{w.r.t.Li} \quad (5)$$

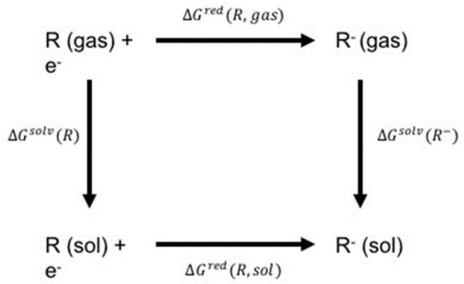

Figure 2. Thermodynamic cycle used to calculate the equilibrium redox potential in the condensed phase.[40, 41]

Reaction conditions for the synthesis of boron-doped-coronenes

Sato and his coworkers suggested a synthetic route for boron-doped carbon nanotubes.[47] We employed their approach to propose a synthetic route for boron-doped coronenes. The synthetic route for one-boron-doped coronene can be defined by

$$4C_{24}H_{12} + 2B_2O_3 + 2Mg \xrightarrow{Inert\ Gas} 4C_{23}BH_{12} + 4CO + 2MgO \quad (6)$$

To determine the pressure condition for the reaction at a given temperature T, we first calculated the standard Gibbs free energy change for the reaction (ΔG^o_T) per mole of the one-boron-doped coronene at 1 atm by

$$\Delta G^o_T = \frac{N_A}{4}\left(4G^0_{C_{23}BH_{12}} + 4G^0_{CO} + 2G^0_{MgO} - 4G^0_{C_{24}H_{12}} - 2G^0_{B_2O_3} - 2G^0_{Mg}\right) \quad (7)$$

where N_A is the Avogadro's constant, which is $6.023 \times 10^{23}\ \mathrm{mol}^{-1}$. $G^0_{C_{23}BH_{12}}$, G^0_{CO}, G^0_{MgO}, $G^0_{C_{24}H_{12}}$, $G^0_{B_2O_3}$, and G^0_{Mg} are the DFT-calculated Gibbs free energies of $C_{23}BH_{12}$, CO, MgO, $C_{24}H_{12}$, B_2O_3 and Mg at a given temperature T and 1 atm, respectively. Then, the Gibbs free energy change for the reaction per mole of the one-boron-doped coronene ($\Delta G_{T,P}$) at a given temperature and pressure can be expressed by

$$\Delta G_{T,P} = \Delta G^o_T + RTln(k) \quad (8)$$

where R is the ideal gas constant, T is the reaction temperature, and k is the equilibrium constant. If the total pressure is maintained at 1 atm and temperature is within a range of *1073.15 K - 1273.15 K*, CO will be the only gaseous phase. Therefore, k can be expressed as

$$k = (P_{CO}/P_{Total})^4 \quad (9)$$

where P_{CO} is the pressure of CO and P_{Total} is the total pressure of the CO and inert gas (assumed to be maintained at 1 atm). Therefore, at an equilibrium state, P_{CO} can be defined by

$$P_{CO} = \sqrt[4]{\exp(-\Delta G_T^o/RT)} \cdot P_{Total} \quad (10)$$

Table 1. The structural symmetry, redox potential, and electron affinity for the pristine coronene and boron-doped coronenes.

Structure				Properties	
Dopant(s)		Case	Existence of reflection line	Redox potential (V vs. Li/Li^+)	Electron affinity (kcal/mol)
Number	Location(s)				
0		P	Yes	0.67	-11.15
1	edge	B1-1	No	5.42	-119.26
	corner	B1-2	Yes	5.30	-117.07
	center	B1-3	Yes	5.28	-115.96
2	edge + edge	B2-1	Yes	2.61	-52.84
		B2-2	No	2.92	-61.89
		B2-3	Yes	3.57	-77.95
		B2-4	No	3.06	-65.81
		B2-5	Yes	-0.39	15.24
		B2-6	No	0.42	-5.82
		B2-7	Yes	0.46	-5.15
		B2-8	Yes	0.38	-3.81
		B2-9	Yes	1.45	-31.37
	edge + corner	B2-10	No	3.00	-63.39
		B2-11	No	3.28	-72.29
		B2-12	No	2.95	-64.21
		B2-13	No	3.07	-66.77
		B2-14	No	2.79	-59.54
		B2-15	No	3.13	-67.00
	corner + corner	B2-16	Yes	0.50	-4.71
		B2-17	Yes	1.82	-36.18
		B2-18	Yes	0.40	-3.99
	corner + center	B2-19	Yes	1.93	-37.33
		B2-20	No	3.33	-71.78
		B2-21	No	3.10	-66.10
		B2-22	Yes	1.12	-20.47
	center + center	B2-23	Yes	3.81	-81.05
		B2-24	No	4.35	-94.15
		B2-25	Yes	1.37	-24.88
	edge + center	B2-26	No	3.13	-65.98
		B2-27	No	3.16	-67.62
		B2-28	No	3.14	-67.52
		B2-29	No	3.18	-68.97
		B2-30	No	3.25	-70.24
		B2-31	No	2.70	-56.54

Results and discussion

Redox potentials of boron-doped coronenes

We designed a series of boron-doped coronene models with either one or two doped boron atoms replacing carbon in various positions. Figure 1 shows all available models for one- and two-boron-doped coronenes, in which the pristine structure ($C_{12}H_{24}$) is labelled by "P" and the boron-doped structures are labelled by "B*m*-*n*" with *m* representing the number of boron dopants and *n* representing the case number. Considering the symmetry of coronene, three possible configurations are available for the one-boron-doped case: a boron at center, corner and edge, named as "B1-1", "B1-2" and "B1-3", respectively. Expanding, 31 distinctive configurations are available for the two-boron-doped case, which are named as "B2-1" through "B2-31". The calculated redox potentials and electron affinities for all of these structures are listed in Table 1. The redox potential of the pristine coronene is predicted

to be 0.67 V (vs. Li/Li^+), which is in a good agreement with the value of 1.07 V (vs. Li/Li^+) reported by Djurovich et al., indicating the reliability of our computational approach.[48] Note that our previous studies also provide the robustness of our computational approach to predict redox potentials of various organic materials [9, 10, 12, 42, 43].

One-boron-doped coronenes developed by replacing one of the three distinctive carbons in the pristine coronene with a boron exhibit the redox potentials of 5.28 V, 5.30 V and 5.42 V vs. Li/Li^+ for the cases of boron placed at the center, corner and edge positions, respectively. One surprising observation is that one boron doping of the pristine coronene increases the redox potential of coronene by 4.6 - 4.8 V vs. Li/Li^+. Regarding this, Manzhos and coworkers studied the electronic density of states (DOS) for pristine coronene and its boron-doped derivatives.[35] They highlighted that a doped boron atom would create a new unoccupied orbital near the highest occupied molecular orbital (HOMO) of the pristine coronene, leading to the shift of the lowest unoccupied molecular orbital (LUMO) toward the HOMO by more than 2 eV. The reduction of the LUMO of the molecule by the boron-doping process leads to the increase of its redox potential. Thus, one unstable unpaired electron generated by the boron dopant may make the molecule prefer to be reduced. Note that the calculated redox potentials for the three one-boron-doped coronenes are higher than those for conventional transition metal oxides, such as $LiFePO_4$ (3.5 V vs. Li/Li^+),[13, 49] $LiCoPO_4$ (4.8 V vs. Li/Li^+),[13, 49] and $LiCoO_2$ (3.9 V vs. Li/Li^+),[49] and those for most organic materials, such as phenalenyl derivatives (~3.93 V vs. Li/Li^+),[43] anthracene derivatives (~3.82 V vs. Li/Li^+),[43] and naphthalene diimide derivatives (2.3-2.9 V vs. Li/Li^+),[19] which demonstrates the promising potential of the boron-doping to enhance the redox potentials of organic materials. In addition, the redox potential is predicted to increase as a function of the distance from the molecular center, exhibiting the highest value (5.42 V vs. Li/Li^+) for the case that a boron is placed at the edge position. Previous experimental studies on cathode materials consisting of graphene/ceramic oxide composites highlighted that graphenes and graphene flakes would not be self-decomposed under high cell voltages (4.7 - 4.8 V vs. Li/Li^+).[50-52] Thus, it is reasonably assumed that coronene and its derivatives, model structures of graphene flakes, would not be self-decomposed under high voltages around 4.8 V vs. Li/Li+ or even above. The possible issue for the oxidation of electrolyte due to such a high potential can be also resolved by employing solid electrolytes or ionic liquids with wide voltage windows.

Redox potentials for 31 two-boron-doped coronenes designed by the additional substitution of a carbon atom in a one-boron-doped coronene by another boron atom exhibit different behaviors from those for the aforementioned one-boron-doped coronenes. As shown in Table 1, their redox potentials vary from -0.39 to 4.35 V vs. Li/Li^+ significantly depending on the positions of doped boron atoms and their separation distances. It is noteworthy that none of the two-boron-doped coronenes outperforms the one-boron-doped coronenes in terms of the redox potential. Incorporation of the second boron atom into a one-boron-doped coronene generates another unpaired electron which may be paired with the one unpaired electron in the one-boron-doped coronene. This stabilization effect may be the main resource that makes the two-boron-doped coronenes be difficult to be reduced as compared with one-boron-doped coronenes. Specifically, the 31 structures can be geometrically classified as either symmetric or asymmetric structures according to the existence of reflection lines in the structures (Figure 1 and Table 1). As shown in Figure 3, the symmetric models generally have low redox potentials (<2.0 V) while the asymmetric models generally have high redox potentials (>2.0 V). It is not surprising because the symmetric structures may have more balanced and stable electron distributions in comparison with the asymmetric structures, which makes the former more difficult to be reduced. Note that the four models, namely “B2-1”, “B2-3”, “B2-6”, and “B2-23” do not follow the general correlation described above. This suggests that numerous factors, such as the spin states, in addition to the geometric factor could be important to comprehensively understand the redox potentials of these models. The investigation of the other factors is beyond the scope of this study and will be further investigated in future work.

Table S2 in Supporting Information lists the redox potentials of pristine coronene and its boron-doped derivatives in vacuum and solution phases to describe the contribution of the solvation to the redox potential. It is found that the solvation consistently contributes to the redox potential by 1.48 – 1.71 V vs. Li/Li+, regardless of the molecular structure. This suggests that the effect of the solvent-derived dielectric polarization on the reduction of the organic molecules would be independent on the configuration of boron doped coronene. This is consistently observed from our previous study on the redox properties of quinone derivatives.[10]

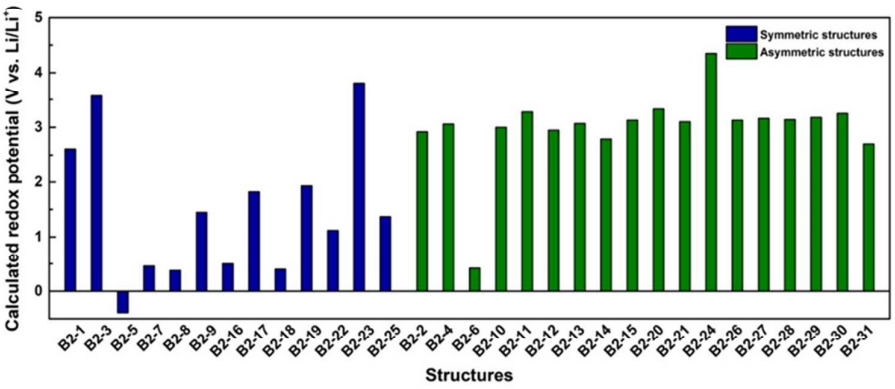

Figure 3. Redox potential of two-boron-doped coronenes classified by their structural symmetry.

The most probable configurations and weight-averaged redox potentials

If we have many number of possible configurations in boron-doped coronenes, which one is probable and which one is not? This question can be answered by evaluating the thermodynamic stability which depends on the geometric positions of boron atoms in the structures. In this study, we attempt to calculate the probability for each configuration of the one- and two-boron-doped coronenes utilizing Boltzmann factor as explained in the previous section.

From the Boltzmann factor analysis in Figure 4a, it is identified that "B1-2" is the only probable configuration for the one-boron-doped coronene case with the probability for its presence close to 100%. The weight-averaged redox potential is therefore predicted to be the same as the redox potential (5.30 V vs. Li/Li$^+$) for "B1-2". Likewise, five configurations out of the 31 two-boron-doped coronenes, namely "B2-14", "B2-16", "B2-31", "B2-18" and "B2-5", are identified to be present with the probabilities of 63.37%, 18.34%, 13.34%, 4.77%, and 0.18%, respectively, for the two-boron-doped coronene case in Figure 4b. Based on the relative probabilities of the five models, the weight-averaged redox potential is estimated to be 2.23 V vs. Li/Li$^+$. Please note that the weight-averaged redox potential for the two-boron-doped coronene case is lower than that for the one-boron-doped coronene case. Nonetheless, it should be highlighted that both cases exhibit the significant improvement of the redox potential as compared with the pristine coronene. This implies the immense potential of lightly boron-doped coronenes as positive electrodes in lithium-ion batteries.

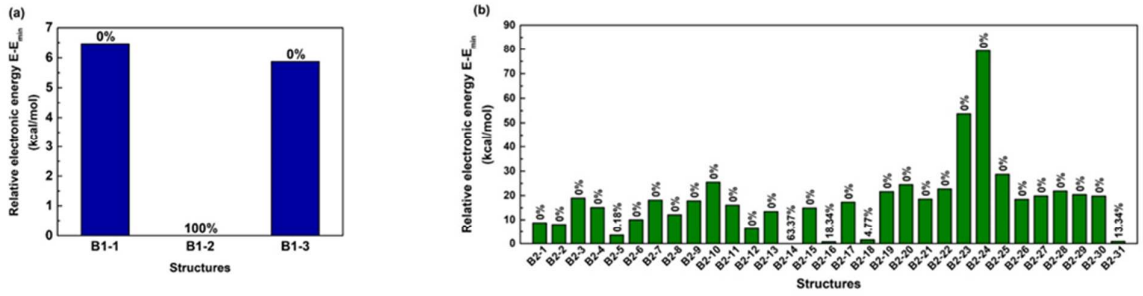

Figure 4. The DFT electronic energies of molecules relative to the most stable molecule for each of (a) one- and (b) two-boron-doped coronenes and their configurational probabilities.

Electronic properties of boron-doped coronenes

The calculated redox potentials for boron-doped coronenes would depend on many factors including the structural variations, mechanical properties (e.g., reduction-induced strain), and electrolyte solvent conditions. However, please note that our primary intention is to find an electronic property that is clearly correlated with the redox potential. To better understand the aforementioned redox properties of the pristine coronene and its boron-doped derivatives, we investigated their electronic properties, such as the electron affinity, LUMO, and HOMO. Figures 5a, 5b, 5c, and 5d show the correlations of the calculated redox potential with the electron affinity, LUMO, HOMO, and the HOMO-LUMO difference, respectively. As expected, the redox potential has a strong linear relationship with the electron affinity (Figure 5a).

Note that the electron affinity is defined by the amount of the free energy released when an electron is added to a neutral molecule. A molecule with more negative value in its electron affinity is more reductive and thus it has higher redox potential. A similar observation has been reported from our previous studies on various organic materials, such as graphene oxides, quinones, dopamines and ketone derivatives.[9, 10, 12, 42, 43] In contrast, the redox potential exhibits a poor correlation with the LUMO energy level (Figure 5b). This is surprising because many previous studies have reported a considerably strong correlation between the redox potential and LUMO energy level.[5, 9, 10, 12, 42, 43] For example, Namazian et al. revealed a strong correlation between the LUMO energy level and redox potential for quinones.[5] Jang and coworkers also reported the similar correlations for graphene oxides,[9, 12] quinones,[10] and dopamines.[42]

To understand the poor correlation between the redox potential and LUMO energy level, we examined total and local spin states for all the molecules studied here. Note that the local spin state addresses the spin state of each atom while the total spin state indicates the sum of the local spin states of all the atoms in a molecule. Table S3 in Supporting Information lists the spin states for the B2-3 case as a representative example. The 31 two-boron-doped structures are classified in three groups based on total and local spin states as displayed in Table 2. The first group, that contains structures with total and local spin states of zero values for both gas and solution phases, has a low tendency on the break-down of paired electrons. The second group contains structures with total and local spin states of zero values for gas phase but non-zero values for solution phase, exhibiting a medium tendency. The last group shows a high tendency because it contains structures with total and local spin states of non-zero values for both gas and solution phases. As expected, considering Table S1 with Table 2 together, the cases with medium or high tendency on the break-down of paired electrons for two-boron-doped coronenes generally became stable at high spin states. Figure 6 shows the degree of the correlation between the redox potential and LUMO energy level for two-boron-doped structures affected by the tendency level. It is observed from the figure that the strong correlation can be predicted from the first group containing the structures with the low tendency on the break-down of paired electrons, indicating that the instability of the local spin states may be the main resource of the weak correlation shown in Figure 5b.

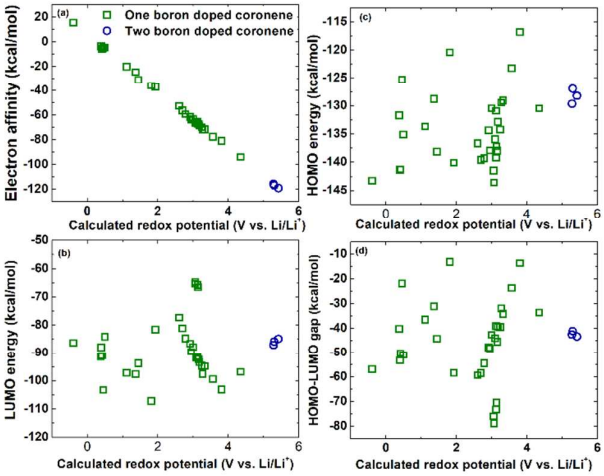

Figure 5. Correlations of the calculated redox potential with (a) the electron affinity, (b) LUMO energy level, (c) HOMO energy level, and (d) HOMO-LUMO gap for one- and two-boron-doped coronenes.

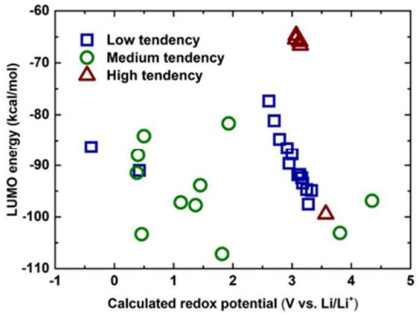

Figure 6. Correlation of the calculated redox potential with the LUMO energy level for two-boron-doped coronenes. They are categorized into three groups according to the tendency on the break-down of paired electrons in terms of total and local spin states.

Thermodynamic feasibility of process for developing boron-doped coronenes

In order to develop practical applications from the boron-doped coronenes, the boron-doping process defined by Equation 6 should be thermodynamically feasible. Figure 7 describes the correlation between the temperature and CO pressure conditions for the boron-doping process at the edge of the coronene. The change of the Gibbs free energy for the reaction defined by Equation 6 becomes negative below the plotted CO pressure at a given temperature. The boron-doping process for one-boron-doped coronene is therefore predicted to be thermodynamically feasible below the plotted CO pressure at a given temperature. As expected, the maximum CO pressure increases with increasing the reaction temperature, exhibiting the gradual increase of the maximum CO partial pressure from 1.3×10^{-6} atm to 2.8×10^{-5} atm as the temperature increases from 1073 K to 1273 K. The CO pressure range required for the boron-doping process is achievable under the inert gas environment (e.g., Ar). This computational analysis

sheds an insight on synthesizing boron-doped coronenes in economic and scalable routes.

Table 2. Spin states of two-boron-doped coronenes in both gas and solution phases. Total and local spin states describe the number of unpaired electrons in systems. The spin states of zero, one, and two indicate singlet, doublet, and trplet, respectively.

Case	Gas phase		Solution phase		Tendency on the break-down of paired electrons
	Total spin states	Local spin states	Total spin states	Local spin states	
B2-1	0	0	0	0	low
B2-2	0	0	0	0	low
B2-3	0	non-zero	2	non-zero	high
B2-4	2	non-zero	2	Non-zero	high
B2-5	0	0	0	0	low
B2-6	0	0	0	0	low
B2-7	0	0	2	Non-zero	medium
B2-8	0	0	0	Non-zero	medium
B2-9	0	0	0	Non-zero	medium
B2-10	0	0	0	0	low
B2-11	0	0	0	0	low
B2-12	0	0	0	0	low
B2-13	2	Non-zero	2	Non-zero	high
B2-14	0	0	0	0	low
B2-15	0	0	0	0	low
B2-16	0	0	0	Non-zero	medium
B2-17	0	0	2	Non-zero	medium
B2-18	0	0	0	Non-zero	medium
B2-19	0	0	0	Non-zero	medium
B2-20	0	0	0	0	low
B2-21	0	0	0	0	low
B2-22	0	0	0	Non-zero	medium
B2-23	0	0	2	Non-zero	medium
B2-24	0	0	2	Non-zero	medium
B2-25	0	0	2	Non-zero	medium
B2-26	2	Non-zero	2	Non-zero	high
B2-27	0	0	0	0	low
B2-28	2	Non-zero	0	Non-zero	high
B2-29	0	0	0	0	low
B2-30	0	0	0	0	low
B2-31	0	0	0	0	low

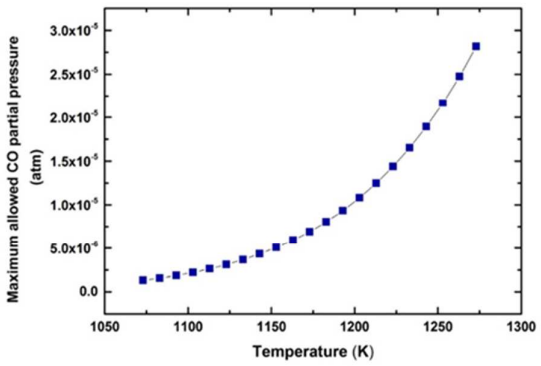

Figure 7. Synthetic conditions for introducing one boron dopant into the pristine coronene under the proposed reaction path. Correlation between temperature and the maximum allowed CO partial pressure within the range of between 1073 K and 1273 K.

Conclusions

In this work, the thermodynamics and redox properties of boron-doped coronones, namely three one-boron-doped and thirty-one two-boron-doped ones, was investigated using well-established density functional theory (DFT) modeling. Pristine coronene with a low redox potential of 0.67 V vs. Li/Li^+, which would be not desirable for positive electrodes in lithium-ion batteries, became redox-active for high-potential lithium-ion batteries through the introduction of boron dopants, exhibiting the weight-averaged redox potentials of 5.30 V vs. Li/Li^+ for one-boron-doped coronenes and 2.23 V vs. Li/Li^+ for two-boron-doped coronenes. The redox potentials of boron-doped coronenes varied with the position and density of the dopant, highlighting the highest redox potential of

5.42 V vs. Li/Li^+ for the coronene with a boron atom doped at an edge position. To the best of our knowledge, this redox potential correspond to the highest value for organic materials reported to date. Redox potentials for thirty-one two-boron-doped coronenes with varied configurations generally ranged into two groups depending on their structural symmetry. Molecules with symmetrically positioned boron atoms exhibited low redox potentials (<2.0 V vs. Li/Li^+), being ascribed to the electronic stabilization of symmetric structures, which made them less preferred to be reduced. In contrast, molecules with asymmetric positions of boron atoms showed high redox potentials (>2.0 V vs. Li/Li^+). Further investigation on the electronic properties of the boron-doped coronenes exhibited a strong correlation between the redox potential and electron affinity. In contrast, a poor correlation of the redox potential with the LUMO energy level was predicted possibly owing to the instability of the local spin states caused by the break-down of paired electrons. Last, a modified synthetic route with viable conditions (temperature: 1073 – 1273 K, CO partial pressure: $\leq 1.3\times10^{-6}$ - 2.8×10^{-5} atm) was proposed for the scalable production of boron-doped coronenes.

Acknowledgements

We acknowledge that this research used resources of the Keeneland Computing Facility at the Georgia Institute of Technology, supported by the National Science Foundation under Contract OCI-0910735. This work was also supported by the President's Undergraduate Research Salary Award (PURA) from the Undergraduate Research Opportunities Program (UROP) at Georgia Institute of Technology. This research was supported by Basic Science Research Program through the National Research Foundation of Korea (NRF) funded by the Ministry of Science, ICT & Future Planning (NRF-2017R1A4A1014806).

Keywords: lithium-ion batteries • cathodes • redox potential • density functional theory • boron doping • coronene

References

1. H. S. Chen, T. N. Cong, W. Yang, C. Q. Tan, Y. L. Li and Y. L. Ding, *Prog Nat Sci*, 2009, **19**, 291-312.
2. B. Dunn, H. Kamath and J. M. Tarascon, *Science*, 2011, **334**, 928-935.
3. G. Jeong, Y. U. Kim, H. Kim, Y. J. Kim and H. J. Sohn, *Energy Environ. Sci.*, 2011, **4**, 1986-2002.
4. N. Nitta, F. X. Wu, J. T. Lee and G. Yushin, *Mater Today*, 2015, **18**, 252-264.
5. M. Namazian, H. A. Almodarresieh, M. R. Noorbala and H. R. Zare, *Chem Phys Lett*, 2004, **396**, 424-428.
6. P. G. Bruce, B. Scrosati and J. M. Tarascon, *Angew. Chem. Int. Ed.*, 2008, **47**, 2930-2946.
7. J. Hassoun, S. Panero, P. Reale and B. Scrosati, *Adv. Mater.*, 2009, **21**, 4807-+.
8. M. D. Bhatt and C. O'Dwyer, *Phys. Chem. Chem. Phys.*, 2015, **17**, 4799-4844.
9. S. Kim, K. C. Kim, S. W. Lee and S. S. Jang, *Phys. Chem. Chem. Phys.*, 2016, **18**, 20600-20606.
10. K. C. Kim, T. Y. Liu, S. W. Lee and S. S. Jang, *J. Am. Chem. Soc.*, 2016, **138**, 2374-2382.
11. D. H. Wu, Y. F. Li and Z. Zhou, *Theor Chem Acc*, 2011, **130**, 209-213.
12. T. Y. Liu, K. C. Kim, R. Kavian, S. S. Jang and S. W. Lee, *Chem. Mater.*, 2015, **27**, 3291-3298.
13. J. W. Fergus, *J. Power Sources*, 2010, **195**, 939-954.
14. V. Etacheri, R. Marom, R. Elazari, G. Salitra and D. Aurbach, *Energy Environ. Sci.*, 2011, **4**, 3243-3262.
15. J. Qian, M. Zhou, Y. Cao, X. Ai and H. Yang, *J. Phys. Chem. C*, 2010, **114**, 3477-3482.
16. L.-X. Yuan, Z.-H. Wang, W.-X. Zhang, X.-L. Hu, J.-T. Chen, Y.-H. Huang and J. B. Goodenough, *Energy Environ. Sci.*, 2011, **4**, 269-284.
17. C. Sun, S. Rajasekhara, J. B. Goodenough and F. Zhou, *J. Am. Chem. Soc.*, 2011, **133**, 2132-2135.
18. D. Rangappa, K. D. Murukanahally, T. Tomai, A. Unemoto and I. Honma, *Nano Lett.*, 2012, **12**, 1146-1151.
19. G. S. Vadehra, R. P. Maloney, M. A. Garcia-Garibay and B. Dunn, *Chem. Mater.*, 2014, **26**, 7151-7157.
20. Z. S. Wu, W. C. Ren, L. Xu, F. Li and H. M. Cheng, *ACS Nano*, 2011, **5**, 5463-5471.
21. Y. Q. Teng, H. L. Zhao, Z. J. Zhang, Z. L. Li, Q. Xia, Y. Zhang, L. N. Zhao, X. F. Du, Z. H. Du, P. P. Lv and K. Swierczek, *ACS Nano*, 2016, **10**, 8526-8535.
22. D. C. Marcano, D. V. Kosynkin, J. M. Berlin, A. Sinitskii, Z. Z. Sun, A. Slesarev, L. B. Alemany, W. Lu and J. M. Tour, *ACS Nano*, 2010, **4**, 4806-4814.
23. X. S. Li, W. W. Cai, J. H. An, S. Kim, J. Nah, D. X. Yang, R. Piner, A. Velamakanni, I. Jung, E. Tutuc, S. K. Banerjee, L. Colombo and R. S. Ruoff, *Science*, 2009, **324**, 1312-1314.
24. R. P. Hardikar, D. Das, S. S. Han, K. R. Lee and A. K. Singh, *Phys. Chem. Chem. Phys.*, 2014, **16**, 16502-16508.
25. Y. Y. Liu, V. I. Artyukhov, M. J. Liu, A. R. Harutyunyan and B. I. Yakobson, *J. Phys. Chem. Lett.*, 2013, **4**, 1737-1742.
26. W. Z. a. J. K. X. Fan, *ACS Appl. Mater. Interfaces*, 2012, **4**, 2432-2438.
27. X. Zhao, C. M. Hayner, M. C. Kung and H. H. Kung, *Adv Energy Mater*, 2011, **1**, 1079-1084.
28. H. Shan, D. B. Xiong, X. F. Li, Y. P. Sun, B. Yan, D. J. Li, S. Lawes, Y. H. Cui and X. L. Sun, *Appl Surf Sci*, 2016, **364**, 651-659.
29. S. H. Gao, Z. Y. Ren, L. J. Wan, J. M. Zheng, P. Guo and Y. X. Zhou, *Appl Surf Sci*, 2011, **257**, 7443-7446.
30. X. L. Wang, Z. Zeng, H. Ahn and G. X. Wang, *Appl Phys Lett*, 2009, **95**.
31. H. B. Wang, C. J. Zhang, Z. H. Liu, L. Wang, P. X. Han, H. X. Xu, K. J. Zhang, S. M. Dong, J. H. Yao and G. L. Cui, *J. Mater. Chem.*, 2011, **21**, 5430-5434.
32. A. L. M. Reddy, A. Srivastava, S. R. Gowda, H. Gullapalli, M. Dubey and P. M. Ajayan, *ACS Nano*, 2010, **4**, 6337-6342.
33. C. Uthaisar, D. J. Hicks and V. Barone, *Surf Sci*, 2014, **619**, 105-113.
34. M. Endo, T. Hayashi, S. H. Hong, T. Enoki and M. S. Dresselhaus, *J Appl Phys*, 2001, **90**, 5670-5674.
35. J. Lüder, M. H. Cheow and S. Manzhos, *Phys. Chem. Chem. Phys.*, 2017, **19**, 13195-13209.
36. *Journal*, 2009.
37. C. Adamo, G. E. Scuseria and V. Barone, *J Chem Phys*, 1999, **111**, 2889-2899.
38. C. Adamo and V. Barone, *J Chem Phys*, 1999, **110**, 6158-6170.
39. R. Ditchfield, W. J. Hehre and J. A. Pople, *J Chem Phys*, 1971, **54**, 724-+.
40. P. Winget, C. J. Cramer and D. G. Truhlar, *Theor Chem Acc*, 2004, **112**, 217-227.
41. A. Lewis, J. A. Bumpus, D. G. Truhlar and C. J. Cramer, *J Chem Educ*, 2004, **81**, 596-604.
42. T. Liu, K. C. Kim, B. Lee, Z. M. Chen, S. Noda, S. S. Jang and S. W. Lee, *Energy Environ. Sci.*, 2017, **10**, 205-215.
43. J. H. Park, T. Y. Liu, K. C. Kim, S. W. Lee and S. S. Jang, *ChemSusChem*, 2017, **10**, 1584-1591.
44. D. J. Tannor, B. Marten, R. Murphy, R. A. Friesner, D. Sitkoff, A. Nicholls, M. Ringnalda, W. A. Goddard and B. Honig, *J. Am. Chem. Soc.*, 1994, **116**, 11875-11882.
45. W. A. Donald, R. D. Leib, J. T. O'Brien, M. F. Bush and E. R. Williams, *J. Am. Chem. Soc.*, 2008, **130**, 3371-3381.
46. S. P. Ong, V. L. Chevrier, G. Hautier, A. Jain, C. Moore, S. Kim, X. H. Ma and G. Ceder, *Energy Environ. Sci.*, 2011, **4**, 3680-3688.
47. W. Q. Han, Y. Bando, K. Kurashima and T. Sato, *Chem Phys Lett*, 1999, **299**, 368-373.
48. P. I. Djurovich, E. I. Mayo, S. R. Forrest and M. E. Thompson, *Org. Electron.*, 2009, **10**, 515-520.
49. D. Andre, S. J. Kim, P. Lamp, S. F. Lux, F. Maglia, O. Paschos and B. Stiaszny, *J. Mater. Chem. A*, 2015, **3**, 6709-6732.
50. L. Liu, H. Zhang, X. Chen, L. Fang, Y. Bai, R. Liu and Y. Wang, *J. Mater. Chem. A*, 2015, **3**, 12320-12327.
51. L. Xiong, Q. Long, Y. Wang, Y. Xiang, X. Wu and Z. He, *Ceram. Int.*, 2016, **42**, 14141-14147.
52. S. J. R. Prabakar, Y.-H. Hwang, B. Lee, K.-S. Sohn and M. Pyo, *J. Electrochem. Soc.*, 2013, **160**, A832-A837.

Graphical abstract